Development of X-ray Fourier Ptychography Using Mirror-based Achromatic X-ray Microscope

Toshiki Ito[1], Takato Inoue[1], Shinnosuke Kurimoto[1], Yuto Tanaka[2]
Yoshiki Kohmura[3], Makina Yabashi[3], and Satoshi Matsuyama[1,2,4,#]

1 Department of Materials Physics, Graduate school of Engineering, Nagoya University, Furo-cho, Chikusa-ku, Nagoya, Aichi, 464-8603, Japan
2 Department of Precision Science and Technology, Graduate school of Engineering, Osaka University, 2-1, Yamadaoka, Suita, Osaka, 565-0871, Japan
3 RIKEN SPring-8 Center, 1-1-1, Kouto, Sayo-cho, Sayo-gun, Hyogo, 679-5148, Japan
4 Research Center for Crystalline Materials Engineering, Graduate school of Engineering, Nagoya University, Furo-cho, Chikusa-ku, Nagoya, Aichi, 464-8603, Japan
Corresponding Author / Email: matsuyama@mp.pse.nagoya-u.ac.jp, TEL: +81-52-789-4683

KEYWORDS: X-ray microscopy, X-ray mirror, advanced Kirkpatrick–Baez mirror, Fourier ptychography

X-ray microscopy enables unique observations based on the short wavelength and high transmittance of X-rays. Furthermore, achromatic and highly efficient observations can be realized using total-reflection mirrors. However, improving the spatial resolution is challenging. First, spatial resolutions beyond the diffraction limit, which depend on the numerical aperture of the objective, cannot be achieved. Second, residual shape errors on mirrors that occur during fabrication are inevitable, thus resulting in optical aberrations and degraded spatial resolutions. Hence, we apply Fourier ptychography (FP) to X-ray microscopy. FP is a technique that improves spatial resolution by applying a special phase retrieval algorithm to multiple images acquired by scanning the illumination angle. We demonstrate the application of X-ray FP using an achromatic X-ray microscope based on total-reflection mirrors. Images of a test chart are successfully reconstructed and a high spatial resolution of 22 nm (half period), which exceeds the diffraction limit of 43 nm (half period) of the objective used, is achieved.

1. Introduction

Due to the short wavelength and high transmittance of X-rays, X-ray microscopy allows us to observe the interior of thick samples at the nanoscale without destruction. Furthermore, X-ray microspectroscopic imaging is realizable when total-reflection mirrors that can provide high throughput and achromaticity are used as the objective[1].

However, improving the spatial resolution of mirror-based X-ray microscopy is challenging. Generally, spatial resolution is inversely proportional to the numerical aperture (NA) of the objective. Increasing the NA is difficult because X-rays cannot be reflected efficiently at large grazing incidence angles. This is because the refractive index of materials in the X-ray region is approximately 0.99999. Consequently, the achievable spatial resolution under practical conditions is limited to approximately 40 nm. In addition, even when state-of-the-art manufacturing techniques are adopted, slight shape errors of only a few nanometers on mirrors are inevitable, thus resulting in optical aberrations and degraded spatial resolutions.

Hence, we applied Fourier ptychography (FP)[2], which is a coherent diffraction imaging technique, to X-ray microscopy. Although FP is typically used in the visible-light field to observe samples with a large field-of-view and high spatial resolution, it is rarely utilized in the X-ray field[3]. A specific phase-retrieval algorithm, as described below, was applied to multiple microscope images acquired while the illumination angle was scanned. This algorithm increases the NA by simultaneously synthesizing apertures and separating aberrations derived from the objective. Therefore, FP is expected to improve spatial resolutions by addressing both NA and aberration problems in X-ray microscopes.

In this study, we develop an X-ray FP system using an achromatic X-ray microscope based on advanced Kirkpatrick–Baez (AKB) mirrors[4] at SPring-8, which is a synchrotron radiation facility. In addition, a method for correcting unintended image shifts caused by camera misalignment during iterative phase-retrieval calculations is proposed. The reconstructed images achieve a high spatial resolution of 22 nm (half-period), which exceeded the diffraction-limit resolution estimated from the NA of the objective mirrors.

2. Fourier ptychography

When a plane wave light perpendicularly incident to a sample is scattered by the sample, the scattered light can be described by the Fourier transform. Under practical conditions, a portion of the scattered light is captured by the lens. Subsequently, the direction and phase of

the light are modulated by the lens. The function of the lens can be described via the inverse Fourier transform. After the light propagates to the camera plane, a wavefield almost identical to that at the back of the sample is formed, which is known as image formation. When the illumination angle is changed from a right angle, the direction of the scattered light changes accordingly, as shown in Fig. 1. Consequently, the lens captures scattered light at different angles derived from spatial frequencies different from those in the case of perpendicular incidence. Therefore, a different image is presented. In addition, sample information with high spatial frequency, which cannot be captured by perpendicular incidence, can be visualized.

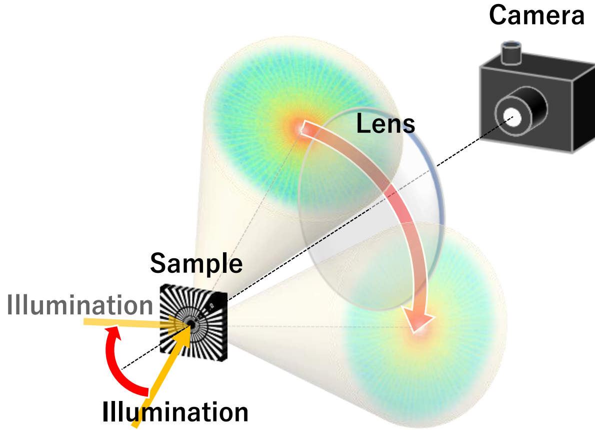

Fig. 1 Schematic illustration of FP. Direction of scattered light changes with illumination angle

In FP, when the illumination angle is scanned, a microscopic image is acquired at each angle. To ensure the uniqueness of the solution, the illumination angle to be scanned is determined such that the scattered light captured by the lens overlaps.

The reconstruction algorithm is briefly explained as follows[5]: The wavefield on the lens plane at the nth iteration and jth illumination angle can be written as

$$\psi_{n,j}(\boldsymbol{u}) = O_n(\boldsymbol{u} - \boldsymbol{u}_j)P_n(\boldsymbol{u}) \tag{1}$$

where $\boldsymbol{u}$ and $\boldsymbol{u}_j$ are the scattering vector and the shift of the scattered light on the lens surface corresponding to changes in the illumination angle, respectively. The wavefield on the camera plane $\phi_{n,j}(\boldsymbol{r})$, i.e., the image formed in a real space with coordinate $\boldsymbol{r}$, is generated by the inverse Fourier transform of $\psi_{n,j}$.

$$\phi_{n,j}(\boldsymbol{r}) = \mathcal{F}^{-1}[\psi_{n,j}(\boldsymbol{u})] \tag{2}$$

Subsequently, only the amplitude of $\phi_{n,j}$ is replaced by the square root of the intensity $I_j(\boldsymbol{r})$ of the captured image at the j th illumination angle. This is the real-space constraint.

$$\phi'_{n,j}(\boldsymbol{r}) = \sqrt{I_j(\boldsymbol{r})}\frac{\phi_{n,j}}{|\phi_{n,j}|} \tag{3}$$

The Fourier transform of $\phi'_{n,j}$ yields the updated wavefield $\psi'_{n,j}(\boldsymbol{u})$.

$$\psi'_{n,j}(\boldsymbol{u}) = \mathcal{F}[\phi'_{n,j}] \tag{4}$$

The ePIE algorithm[6], which his typically used in ptychography[7], allows O and P to be updated individually while O and P are separated from $\psi_{n,j}$ and $\psi'_{n,j}$ as follows:

$$O_{n+1}(\boldsymbol{u}) = O_n(\boldsymbol{u}) + \alpha\frac{P_n^*(\boldsymbol{u}+\boldsymbol{u}_j)}{|P_n(\boldsymbol{u}+\boldsymbol{u}_j)|^2_{max}}\left(\psi'_{n,j}(\boldsymbol{u}) - \psi_{n,j}(\boldsymbol{u})\right) \tag{5}$$

$$P_{n+1}(\boldsymbol{u}) = P_n(\boldsymbol{u}) + \beta\frac{O_n^*(\boldsymbol{u}-\boldsymbol{u}_j)}{|O_n(\boldsymbol{u}-\boldsymbol{u}_j)|^2_{max}}\left(\psi'_{n,j}(\boldsymbol{u}) - \psi_{n,j}(\boldsymbol{u})\right) \tag{6}$$

At the next illumination angle $j+1$, a new wavefield $\psi_{n,j+1}(\boldsymbol{u})$ is obtained using the updated O and P. The overlap with O in the previous illumination angles, which is the reciprocal space constraint, can serve as an important information.

As the iterative calculations above are repeated, O and P eventually converge to solutions that satisfy the two constraints and the experimental data. Finally, we can obtain the sample's complex transmittance o with improved spatial resolution because the reconstructed o contains no blur, owing to the separation of P, and has a wide, large spatial frequency range owing to all the acquired images with different illumination angles.

3. Experiment

We performed a proof-of-concept experiment to demonstrate the X-ray FP using a mirror-based X-ray microscope at SPring-8. Although FP requires the illumination angle to be scanned, tilting the incident X-rays provided by large synchrotron radiation facilities is impractical. Therefore, in this experiment, the illumination angle was varied by tilting the microscope instead of using a light source. The experimental setup is shown in Fig. 2. The sample and objective mirrors were placed on the same stage system, which can be tilted by rotation and translation stages, while the rotation center on the sample was maintained. Only the camera was placed at different translation stages because it was placed distant from the mirrors. However, the translation stage at the bottom of the camera allows tracking of the moving x-ray image as the illumination angle changes.

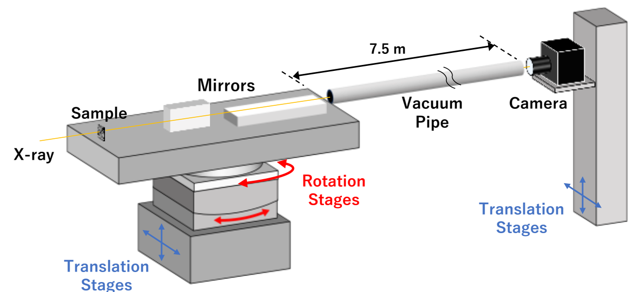

Fig. 2 Experimental setup. Mirrors and sample are placed on the same stage to tilt the entire system. Camera is placed on the other stage and can monitor the shift in the image based on the tilt of the stage for the mirrors and sample.

AKB mirrors, which comprise four reflection mirrors, were used as the reflective objective lenses in the X-ray microscope. The NAs were1.51 and 1.44 mrad in the horizontal and vertical directions, respectively. A fine test chart constructed using Ta (NTTAT, XRESO-20) with a minimum feature size of 20 nm was used as the sample.

The incident X-ray energy, which was 9.884 keV, was monochromatized using a double-crystal monochromator. The illumination angle was scanned over a range of ±1.0 mrad at a scanning step of 0.11 mrad. A total of 361 (19 × 19) X-ray images were captured at an exposure time of 5 s/image.

4. Correction of Misalignment of Camera

The camera was shifted separately from the mirrors and sample, and each scan caused a misalignment in their relative positions (Fig. 3). Although the illumination angle was accurately monitored by the autocollimator, the camera, which was positioned 7.5 m away from the sample, deviated slightly and randomly owing to stage motion errors. Because fluctuating X-ray images cause fatal calculation errors, they should be corrected precisely to obtain a high-quality reconstruction.

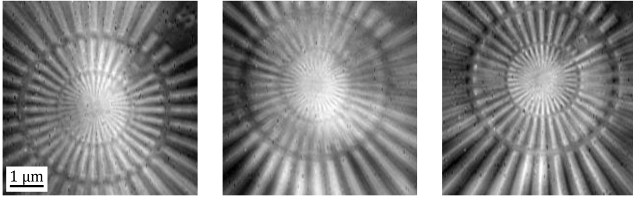

Fig. 3 Fluctuated X-ray image caused by motion error of translation stages used

We eliminated this misalinment during the phase retrieval calculation by applying a method[8] similar to one that is typically used in ptychography. The procedure was as follows: First, a cross-correlation function $C(\Delta x, \Delta y)$ was obtained between the square root of the captured image $\sqrt{I_j(x,y)}$ and the amplitude of the estimated wavefield on the camera plane $\phi_{n,j}(x,y)$.

$$C(\Delta x, \Delta y) = \sum_{x,y} \sqrt{I_j(x,y)} \cdot |\phi_{n,j}(x-\Delta x, y-\Delta y)| \qquad (7)$$

The position shift of $(\Delta x, \Delta y)$, where the maximum $C(\Delta x, \Delta y)$ can be obtained, is defined as the estimated misalignment. The position shift of the captured image is used to correct the misalignment.

$$I'_j(x', y') = I_j(x-\Delta x, y-\Delta y) \qquad (8)$$

This correction was introduced before imposing real-space constraints at each illumination angle. As O and P were gradually reconstructed, the sample position in the experimental data converged to an accurate position.

5. Results

Fig. 4(a) shows the captured image when the X-rays were perpendicularly incident. Before the reconstruction, the image was blurred owing to the optical aberration of the AKB mirror. Fig. 4(b) shows the phase distribution image of the sample (phase of o) after reconstruction using the FP phase-retrieval calculation. During the reconstruction, the misalignment of the sample images for each illumination angle was successfully corrected with subpixel accuracy using the correction method. The separated optical aberration, i.e., the phase of the reconstructed P, is shown in Fig. 4(c).

Compared with the captured image, the reconstructed image was much clearer and finely resolved. To investigate the spatial resolution comprehensively, the Fourier ring correlation (FRC)[9] was utilized as follows: The captured X-ray images were divided into two groups. And they were reconstructed in the same way. The correlation between the two reconstructed images in the reciprocal space was calculated (Fig. 5), and the estimated spatial resolution was 22 nm (half the period).

The estimated resolution was considered reasonable because the minimum feature of the test chart with a minimum linewidth of 20 nm is just barely visible. Based on the experimental conditions, the diffraction limit of the AKB mirrors was estimated to be $\delta = 0.5\lambda/NA \approx$ 43 nm (half period) based on the Abbe diffraction limit. Therefore, we demonstrated that FP successfully improved the spatial resolution beyond the diffraction limit.

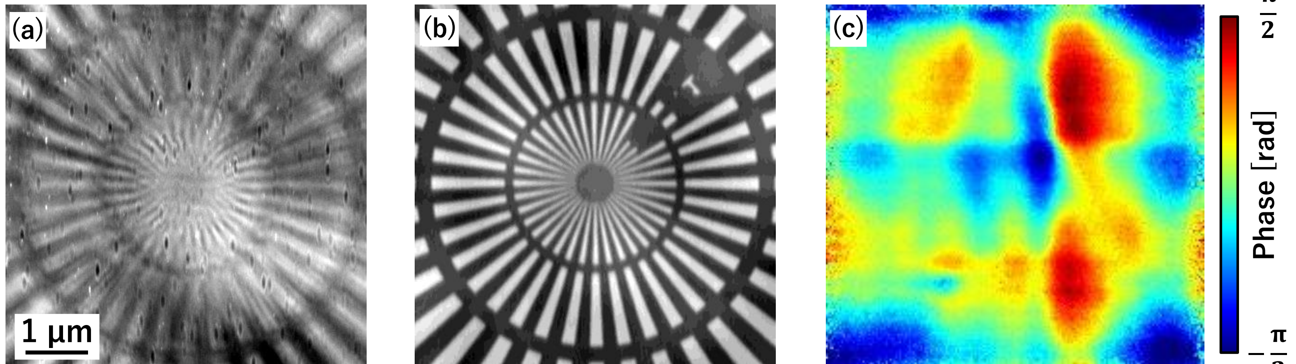

Fig. 4 (a) Microscope image acquired at perpendicular incident angle. (b) Reconstructed phase distribution of the sample (phase of $\boldsymbol{o}$). (c) Reconstructed phase of optical aberration (phase of $\boldsymbol{P}$).

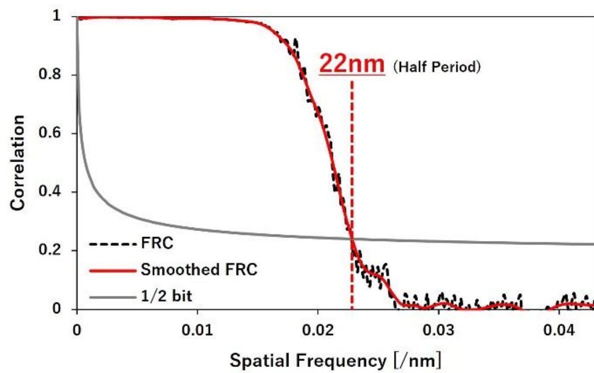

Fig. 5 Result of FRC; 1/2 bit curve[10] was used as threshold to determine the achievable spatial resolution.

6. Conclusions

In this study, we developed a dedicated measurement system and misalignment correction algorithm to apply FP to an achromatic X-ray microscope equipped with total-reflection mirrors. The result of an X-ray FP experiment conducted at SPring-8 indicated the achievement of a spatial resolution of 22 nm (half period), which exceeded the diffraction limit of 43 nm (half period), as calculated from the NA of the reflective lens.

ACKNOWLEDGEMENT

This study was financially supported by Fusion-Oriented REsearch for Disruptive Science and Technology (JPMJFR202Y) and the Japan Society for the Promotion of Science (JP17H01073, JP21H05004, and JP22H03866). The use of B29XUL at SPring-8 was supported by RIKEN.

REFERENCES

1. Matsuyama, S., et al., "Full-field X-ray fluorescence microscope based on total-reflection advanced Kirkpatrick–Baez mirror optics," Opt. Express., Vol. 27, No. 13, pp. 18318-18328, 2019.
2. Zheng, G., Horstmeyer, R., Yang C., et al., "Wide field, high resolution Fourier ptychographic microscopy," Nat. Photonics., Vol. 7, No. 9, pp. 739-745, 2013.
3. Wakonig, K., et al., "X-ray Fourier ptychography," Sci. Adv., Vol. 5, No. 2, 2019
4. Matsuyama, S., et al., "50-nm-resolution full-field X-ray microscope without chromatic aberration using total-reflection imaging mirrors," Sci. Rep. Vol. 7, No. 1, 46358, 2017.
5. Ou X., Zheng G., Yang C., "Embedded pupil function recovery for Fourier ptychographic microscopy," Opt. Express., Vol. 22, No. 5, pp. 4960-4792, 2014
6. Maiden, A. M., Rodenburg, J. M., "An improved ptychographical phase retrieval algorithm for diffractive imaging," Ultramicroscopy, Vol. 109, No. 10, pp. 1256-1262, 2009.
7. Rodenburg, J. M., Faulkner, H. M. L., "A phase retrieval algorithm for shifting illumination," Appl. Phys. Lett., Vol. 85, No. 20, pp. 4795-4797, 2004.
8. Diaz, A., et al., "Translation position determination in ptychographic coherent diffraction imaging," Opt. Express. Vol. 21, No. 11, pp. 13592-13606, 2013.
9. Banterle, N., et al., "Fourier ring correlation as a resolution criterion for super-resolution microscopy," J. Struct. Biol., Vol. 183, No. 3, pp. 363-367, 2013.
10. Heel, M. V., Schatz, M., "Fourier shell correlation threshold criteria," J. Struct. Biol, Vol. 151, No. 3, pp. 250-262, 2005.